Modeling of hard turning: effect of tool geometry on cutting force

Z.Y. Shi[1,a], Z.Q. Liu[1,a], C.M. Cao[1,a]
[1] School of Mechanical Engineering, Shandong University, Jinan250061, China
[a] Key Laboratory of High Efficiency and Clean Mechanical Manufacture (Shandong University), Ministry of Education

Abstract. Hard machining for manufacturing dies and molds offers various advantages, but the productivity is often limited, mainly by tool life. This study investigates the influence of cutting tool geometry on the cutting forces by utilizing finite element simulations (FEM). A set of cutting conditions in numerical FEM were conducted by using four different shaped cutting tools and axial force, radial force and tangential force were found. The results of this research help to explain the conclusion that for cylindrical control, the equation of the actual geometry of the S-shaped inserts involved in cutting is a sphere; that of C-shaped, D-shaped and T-shaped inserts involved in cutting is an ellipsoid with different lengths of short-half axis.

Keywords: tool geometry, material flow stress, short-half-axial, cutting force

1. Introduction

The most common manufacturing process in industry is cutting [1], and FEM has become a major tool in calculating the cutting process variables such as forces, temperatures and stresses [2]. The hard turning of ferrous metal parts that are hardened usually between 45-70 HRC, can be performed dry using ceramic coating tools. In macro machining, the primary cutting edge mainly participates in the cutting process. However, the whole nose of the cutting tool participates in a micro-cutting process due to the metal removed is very little [3]. The cutting force in cutting processes is very important for analyzing the effect of the tool geometry, and there are three different approaches for calculating the forces including: analytical, mechanistic, and numerical [4]. The advantages of using numerical simulation is the cutting forces can be predicted without spending time and money with experimental procedures, therefore improving productivity and reducing costs [1, 5].

In this work, DEFOERM-3D was used to simulate the turning process and the effects of tool geometry parameters on cutting forces in micro-cutting were predicted. Results of the research help to explain the conclusion that for cylindrical control. The equation of the actual geometry of the S-shaped inserts involved in cutting is a sphere, while that of C-, D-, and T-shaped inserts involved in cutting is an ellipsoid with different lengths of short-half axis.

2. Geometry modeling

In traditional machining, the actual geometry of the cutting tool involved is determined by the major cutting edge. In micromachining, in contrast, the actual geometry involved in machining is determined by the major cutting edge, the minor cutting edge and the third edge called the back-side cutting edge. So the cutting tool's nose radius, cutting edge radius etc. have to be considered.

According to ISO code, the tool geometry can be divided into S-, C-, T- shapes etc according to the tool nose angle α. In this paper, four different cutting tools C-, D-, T- and S-shapes tools are selected, meaning the tool angle α is 80º, 55º, 60º, 90º respectively, to investigate the effects of tool geometry on cutting forces.

The cutting tools were also classified into cylindrical control and conical control according to the shape of the flank.

By comprehensively considering the tool shape and the control model of the flank, the cutting tools were classified into four different types including S- and non-S-shaped tools with cylindrical control and conical control. In this paper, because of the limitation of experiments, only S- and non-S-shaped tools with cylindrical control tools are discussed.

In this paper, the model of the actual geometry of the cutting tools involved in machining are developed by using mathematical analysis methods. First, three-dimensional models of the tool nose and major and minor cutting edges are established. Then the transformation matrixes from local coordinate system to global coordinate system are described. Finally the solving processes are carried out and the actual geometry involved in machining is obtained [6]. For S shape tools, the actual geometry involved in machining is a sphere, which is now given in Eq. 1:

$$\left(x-\frac{P}{2}\right)^2+\left(y-\frac{Q}{2}\right)^2+z^2=\frac{R^2+r_1^2+r_2^2}{2}-\frac{Q^2+P^2}{4} \quad (1)$$

where P is the distance between the coordinate system centre of the side cutting edge to the tool nose centre in X direction, Q is the distance between the coordinate system centre of the main cutting edge to the tool nose centre in Y direction, R is the nose radius, r_1 is the major cutting edge radius, and r_2 is the minor cutting edge radius.

For non-S-shaped tools, such as C-, D-, T-shape tools, the actual geometry involved in cutting can be expressed as shown in Eq. 2. According to Yao [7], the projection of the actual geometry of cylindrical control inserts with non-S shape involved in machining in x-y plane is an ellipse, so the 3-D geometry involved in machining is ellipsoid.

$$\begin{cases}\left(2-\cos^2\frac{\alpha}{2}\right)x^2+\left(2-\sin^2\frac{\alpha}{2}\right)y^2+2\sin\frac{\alpha}{2}\cos\frac{\alpha}{2}xy=R^2+r_2^2-r_1^2\\ z=t\end{cases} \quad (2)$$

where α is the tool nose angle.

Fig. 1 shows the actual geometry depicted by Matlab 7.0 according to Eqs. 1 and 2; where Fig. 1a shows the S-shaped tools, 1b shows the C-shaped tools, 1c shows the D-shaped tools, and 1d shows the T-shaped tools, both the major and the minor cutting edge radii are set to be 0.04 mm, and the tool nose radius is set to be 0.2 mm. It can be seen that the three-dimensional graphics of 1a shows a sphere, and the second half of 1b, 1c and 1d are all ellipsoids which gives good consistency Eq. 1 and Eq. 2. By analyzing the three graphics of Fig. 2b, 2c and 2d, it can be seen that length of the short-half-axis of the ellipsoids are different according to the shape of the cutting tools. The longest short-half-axis corresponds with D-shaped tool, whose tool nose angle is 55º, then comes the T-shaped tool, with a tool nose angle of 60º, and finally comes the C-shaped tool, with a tool nose angle of 80º. So, the conclusion can be drawn that with an increase in the tool nose angle, the short-half-axis of the ellipsoid determined by the tool cutting edge and tool nose decrease.

3. Computer Simulation

3.1 Modeling of Workpiece

Bars of stainless steel AeroMet100, 55 mm in diameter and 60º arc-types were used, as shown in Fig. 2. During the FEM simulation process, the main problem is considering the flow stress of the workpiece. According to Yang [8], when the material's strain rate is $10s^{-1}$, the strain-stress curves in 950º, 1000º, 1050º, 1100º can be derived and by using the material property manager, enabling Fig. 3 to be finally derived. Thus, the property of the new material AeroMet100 can be added into the software, and this makes the simulation results more exact.

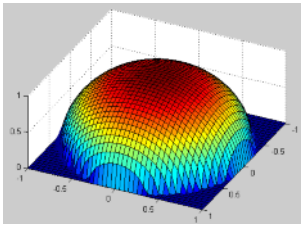

a

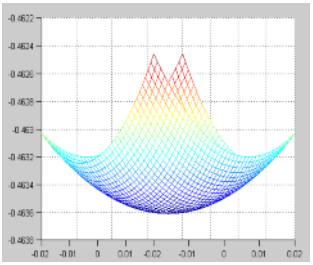

b

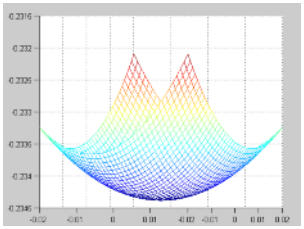

c

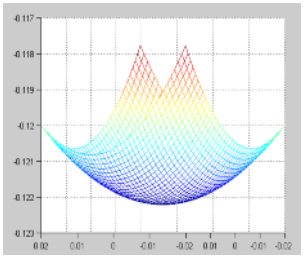

d

Fig. 1. Three-dimensional graphics of actual geometry a. Sketch map of S-shaped tool; b. Sketch map of C-shaped tool; c. Sketch map of D-shaped tool; d. Sketch map of T-shaped tool

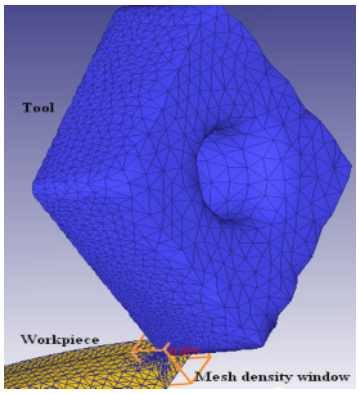

Fig. 2. Cutting process model

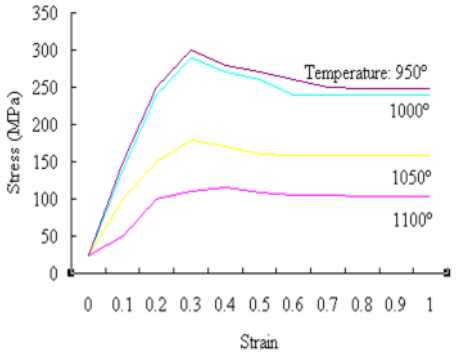

Fig. 3. Flow stress data of AeroMet100

3.2 Contact Friction Model & Heat Transformation

The relationship between the cutting tool and the workpiece was set to be a Master-slave relationship, making sure that the workpiece material will not soak into the cutting tool.

Fig. 4 shows the main view of the cutting process. It can be seen that the chip area was varies along the tool nose from the feed rate to zero, and there must exist an intermediate value which is equal to the nose radius. When the chip area is smaller than the nose radius, no chip come into being, and only a rubbing action occurs during the cutting process. Meanwhile, when the chip area is larger than the nose radius, a chip will be produced and shearing action occurs during the cutting process. So the chip area can be divided into a rubbing area and a shearing area, and the friction model has to be considered seriously. In this paper, for simplicity, the friction model between the cutting tool and the chip is characterized as a shear friction model with the friction coefficient set to be 0.2 [9].

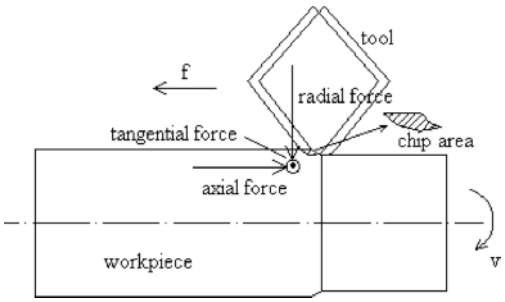

Fig. 4. Main view of the cutting process

The room temperature of the cutting tool and workpiece was set to be 20º, and the coefficient of heat transformation was set to be 11 N/sec/mm/C [10].

The simulation process is shown diagrammatically in Fig. 5.

4. Results and Discussion

Table 1 shows the resulting forces as predicted by the FEM simulation. By analyzing the four shaped tools' resultant forces, it can be concluded that the cutting force generated by the D-shaped tool was substantially higher than the equivalent forces of the other tools. The next highest one was the T-shaped tool, then the C-shaped tool and finally the S-shaped tool. An earlier conclusion was that the longest short-half-axis of the ellipsoid corresponds with D-shaped tool, whose tool nose angle is 55º, the next longest is the T-shaped tool, with tool nose angle is 60º, the next the C-shaped tool, with tool nose angle is 80º, and finally is the S-shaped tool with tool nose angle 90º. These relationships between the cutting forces and the inserts shape have been obtained: the longest of the short-half-axis corresponding to the smallest tool nose angle and the greatest of the cutting forces. This may be due to the ellipsoid with longest short-half-axis having most contact area, which in turn makes heat dissipation better and the cutting temperature lower. When the cutting temperature is reduced, the workpiece material begins to harden, which finally causes the cutting force to increase. By the same token, the magnitude of other cutting tools' cutting forces can be explained and the relationships between the cutting forces and the cutting tools' shape can also be explained.

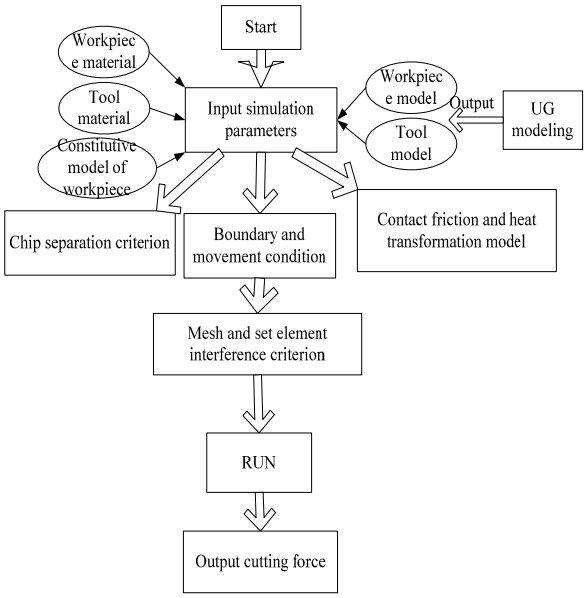

Fig. 5. Flow chart of simulation process

Table 1. Table with legends of one line

Insert type	Simulations		
	Axial force (N)	Radial force (N)	Tangential force (N)
C	39.4	94.2	78.4
D	40.3	101.5	86.2
T	38.1	98.4	84.1
S	32.1	72.6	62.7

5. Conclusions

The following conclusions can be drawn:

1) The simulated model combined with the 3D model built in UG can predict the cutting forces preferable.
2) Different from conventional cutting, in this model the cutting forces in X, Z directions are far higher than the cutting force in the Y(axial) direction.
3) The cutting force of the D-shaped tool was substantially higher than the other shaped tools, the second highest was the T-shaped tool, and then the C-shaped tool and finally the S-shaped tool.
4) The longest of the short-half-axis corresponded with the smallest tool nose angle and gave the greatest of the cutting forces.

Acknowledgement

This project is supported by National Natural Science Foundation of China (through grant no. 50675122 and 50828501), Foundation of Shandong Province of China for Distinguished Young Scholars (2009 JQB01027) and National Basic Research Program of China (973 Program 2009CB724401).

References

[1] Davim JP, Maranhao C, Jackson MJ, Cabral G, Gracio J, (2008) FEM analysis in high speed machining of aluminium alloy (Al7075-0) using polycrystalline diamond (PCD) and cemented carbide (K10) cutting tools. Int. J. Adv. Manuf. Technol. 39: 1093-1100.

[2] Ceretti E, Lazzaroni C, Menegardo L, Altan T, (2000) Turning simulations using a three-dimensional FEM code. J. Mater. Process. Technol. 98: 99-103.

[3] Liu ZQ, (1999) Repetitive measurement and compensation to improve workpiece machining accuracy. Int. J. Adv. Manuf. Technol. 15: 85-89.

[4] Lai XM, Li HT, Li CF, Lin ZQ, Ni J, (2008) Modeling and analysis of micro scale milling considering size effect, micro cutter edge radius and minimum chip thickness. Int. J. Mach. Tools. Manuf. 48: 1-14.

[5] Altintas Y, (2000) Manufacturing automation: Metal cutting mechanics machine tool vibrations and CNC design. Cambridge University Press, Cambridge.

[6] Shi ZY, Liu ZQ, (2009) The actual geometry of the cutting tool involved in machining. Int. J. Adv. Manuf. Technol. (in press, Doi 10.2007/s00170-009-2081-0)

[7] Yao NX, Wang ZH, Chen ZJ, (1988) Application of Math in Tool Design. Mechanical Industry, Beijing.

[8] Yang XH, Zhang SH, (2007) Hot deformation behavior of ultrahigh strength steel AerMer100. Journal of Plasticity Engineering 14: 121-126.

[9] Tang ZT, (2008) Residual stresses and deformations of aerospace aluminum alloy in machining, (Dissertation Shandong University).

[10] Dong HY, (2004) The FEM simulation of overall structure of the aviation in machining, (Dissertation Zhejiang University